

# Bimolecular and Auger Recombination in Phase-Stable Perovskite Thin Films from Cryogenic to Room Temperature and Their Effect on the Amplified Spontaneous Emission Threshold

*Isabel Allegro<sup>1</sup>, Yang Li<sup>1,2</sup>, Bryce S. Richards<sup>1,2</sup>, Ulrich W. Paetzold<sup>1,2</sup>, Uli Lemmer<sup>1,2</sup>, Ian A. Howard<sup>1,2\*</sup>*

<sup>1</sup>Light Technology Institute, Karlsruhe Institute of Technology, Engesserstrasse 13, 76131 Karlsruhe, Germany.

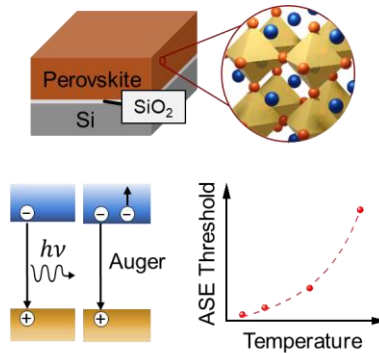
<sup>2</sup>Institute of Microstructure Technology, Karlsruhe Institute of Technology, Hermann-von-Helmholtz-Platz 1, 76344 Eggenstein-Leopoldshafen, Germany.

**Corresponding Author**

\*ian.howard@kit.edu

## ABSTRACT

Recently, continuous-wave (CW) lasing was demonstrated at room temperature in quasi-2D perovskites. For 3D films, CW lasing at room temperature remains challenging. Issues hampering 3D materials include the temperature dependence of the: (a) distribution of carrier energies, (b) build-up of photo-induced non-radiative channels, and (c) rates of bimolecular versus Auger recombination. We study the latter in a phase-stable 3D perovskite using high index substrates to completely suppress amplified spontaneous emission (ASE). The bimolecular recombination coefficient decreases from 80 to 290 K (from  $6.4 \cdot 10^{-10} \text{ cm}^{-3}\text{s}^{-1}$  to  $1.1 \cdot 10^{-10} \text{ cm}^{-3}\text{s}^{-1}$ ), whereas the Auger coefficient stays constant at  $3 \cdot 10^{-29} \text{ cm}^{-6}\text{s}^{-1}$ . Above 250 K, the Auger rate exceeds the bimolecular rate at carrier densities corresponding to the ASE threshold. At lower temperatures, the decrease of the bimolecular rate coefficient with increasing temperature, and the fraction of photoluminescence in the ASE band determine the temperature dependence of the ASE threshold.



Metal halide perovskites have emerged as a promising class of materials for optoelectronic applications, such as lasers and light-emitting diodes.<sup>1</sup> Significant progress has been recently achieved concerning continuous-wave (CW) lasing – a milestone in its own right, and an important step towards the possibility of achieving electrically pumped lasing. CW lasing at room temperature has been demonstrated for low dimensional perovskite systems: in polariton lasing in nanowires<sup>2</sup> and nanoplatelets,<sup>3</sup> and very recently, in exciton lasing in quasi-two-dimensional perovskite thin films fabricated on a distributed feedback structure<sup>4</sup>.

Unambiguous proof of CW lasing at room temperature in three-dimensional (3D) perovskite films, whose emission is based on bimolecular carrier recombination, remains disputed<sup>5,6</sup>. However, Jia *et al.*<sup>7</sup> demonstrated clear proof of CW lasing at 100 K in a mixed-phase perovskite,  $\text{CH}_3\text{NH}_3\text{PbI}_3$  (MAPI), that undergoes an orthorhombic-to-tetragonal phase transition at 160 K. We observed CW amplified spontaneous emission (ASE) at cryogenic temperatures in single-phase perovskite thin films.<sup>8</sup> These films, with the non-stoichiometric chemical composition of  $\text{Cs}_{0.1}(\text{MA}_{0.17}\text{FA}_{0.83})_{0.9}\text{Pb}_{0.84}(\text{I}_{0.84}\text{Br}_{0.16})_{2.68}$ , exhibited CW ASE at temperatures from 80 K to 120 K while still completely in the cubic phase.<sup>9</sup> Our triple cation films show similar ASE behaviour to MAPI at room temperature reported by another group.<sup>10</sup> Here, we investigate the carrier recombination dynamics of this phase-stable triple cation perovskite as a function of temperature to investigate why CW ASE is not achieved at temperatures higher than 120 K. In particular, we determine the second-order carrier recombination coefficient (responsible for radiative decay), and the third-order Auger recombination coefficient (a non-radiative loss channel) as a function of temperature from 80 K to 290 K. Knowing these rates enables the analysis of the influence of Auger recombination in the lasing process.

To accurately determine the Auger rate, we need to measure carrier dynamics after very intense impulsive excitation. Such high-fluence pulsed excitation is above the ASE threshold for thin films prepared on standard substrates (e.g. glass, sapphire). In the case that ASE occurs in the film, the charge carrier concentration becomes clamped. This domination of the dynamics by the ASE process precludes simple extraction of the Auger coefficient. Therefore, we use a silicon (Si) substrate with a higher refractive index ( $n \approx 3.7$  at 770 nm) to eliminate the waveguiding in the perovskite film and completely suppress ASE. The Si is capped with an evaporated 10 nm thin silicon dioxide layer to prevent any possible effects of charge extraction into the substrate. A similar approach was used to study higher-order population dynamics in conjugated polymers.<sup>11</sup>

Figure 1 compares the light-in light-out curves measured under femtosecond excitation for a perovskite film on sapphire ( $n \approx 1.76$  at 770 nm), and on Si ( $n \approx 3.7$  at 770 nm). The reference on the sapphire substrate is the structure that achieves CW ASE at cryogenic temperatures,<sup>9</sup> in which a perovskite thin film with a refractive index of 2.5 (at 770 nm) acts as the core of the slab waveguide and the propagating mode is confined within the perovskite gain medium (Figure 1a). The light-in light-out curves obtained at all temperatures exhibit clear ASE thresholds for these reference samples, whereas no ASE is observed in the analogous samples on the Si substrate (Figures 1c-f). The ASE threshold is evident from the characteristic kink in the light-in light-out curves, along with the distinctive spectral narrowing (Figure S1). In the case of the Si substrate, there is no guided mode in the perovskite since the substrate has the highest refractive index in the stack of 3.7 (Figure 1b). Consequently, the light-in light-out curves of perovskite films on Si do not exhibit the inflection point for ASE but become sublinear at high carrier densities (Figures 1c-f). Also, spectral narrowing is not observed (Figure S1). The Si substrates completely suppress ASE allowing the Auger rate to be accurately determined at high carrier densities.

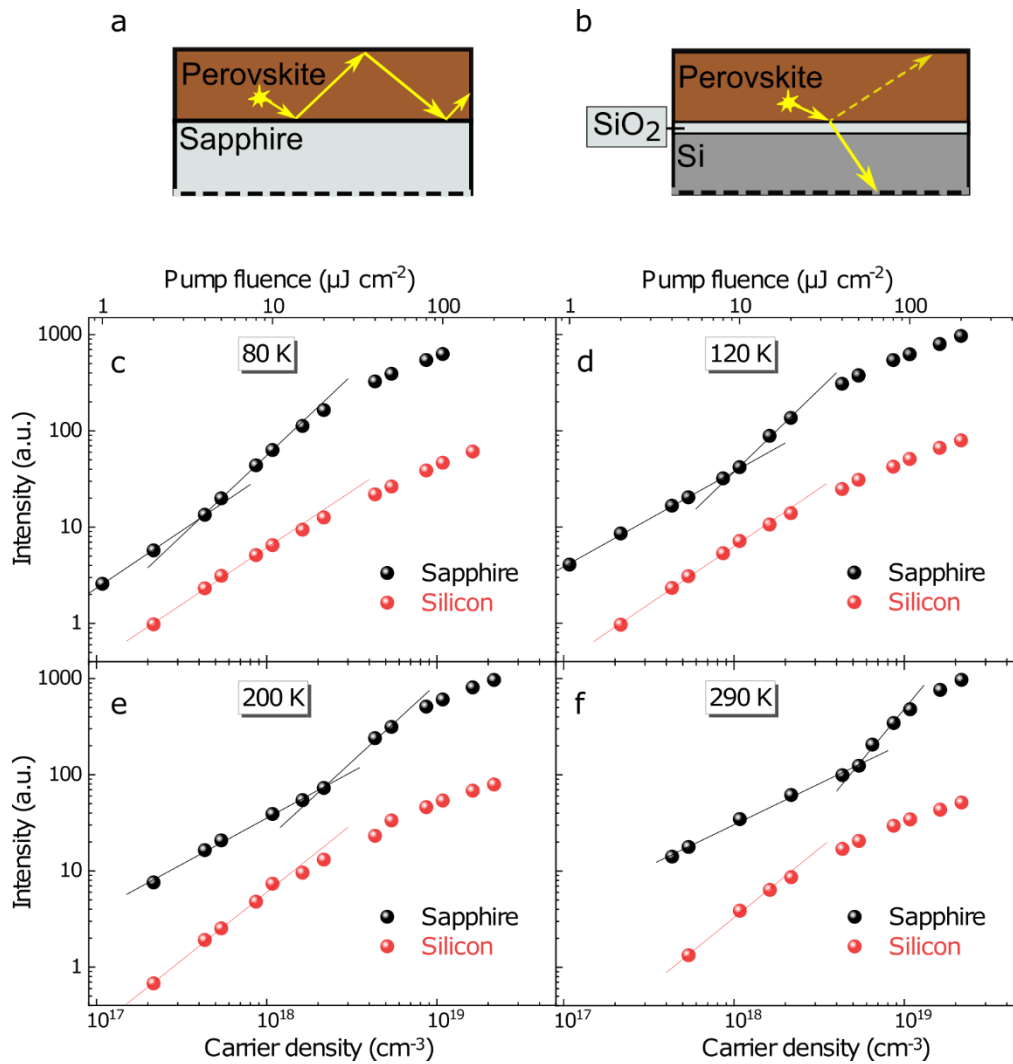


**Figure 1.** Comparison between perovskite films deposited on sapphire and silicon substrates. A perovskite layer on sapphire acts as a waveguide allowing amplified spontaneous emission (ASE) to occur in the layer (a). Conversely, on silicon, light is not guided in the perovskite layer and ASE is completely suppressed (b). Emission intensity as a function of initial carrier density for perovskite layers on the two substrates (vertical offset for clarity) at different temperatures: 80 K (c), 120 K (d), 200 K (e) and 290 K (f). The emission intensity corresponds to the maximum value of the spectrum collected via surface detection. Excitation was with a femtosecond laser (532 nm, 260 fs, 1 kHz). The intersection of the linear fits for the sapphire substrate gives the ASE threshold, whereas the linear fit for the silicon substrate emphasizes the sublinear dependence of the emission intensity on carrier density due to increasing role of Auger recombination.

We use transient reflection spectroscopy (TR) to study the dynamics of the perovskite thin film on a Si substrate and make use of the strong signal in the near infra-red (NIR) region to monitor the charge carrier density as a function of time. This signal reveals the change in refractive index, which is proportional to the concentration of free carriers in the material.<sup>12-17</sup> Exemplary spectra as a function of time are given in Figure S2.

Similar to the temperature-dependent study of Milot *et al.*<sup>18</sup> utilizing visible-pump terahertz-probe spectroscopy to determine the carrier dynamics on MAPI across its different crystal phases, we globally fit TR measurements over a range of excitation fluences for a sequence of temperatures between 80 K and 290 K to extract the temperature-dependent bimolecular and Auger rates.

The charge carrier lifetimes as a function of fluence for different excitation fluences are presented in Figure 2. We neglect the influence of the monomolecular recombination coefficient  $k_1$  in our analysis, as bimolecular and Auger recombination dominate in the fluence range considered (details are provided in the Supporting Information, Figures S4-6).<sup>19</sup> Consequently, the carrier dynamics can be described with the following rate equation

$$\frac{dn(t)}{dt} = -k_2n(t)^2 - k_3n(t)^3 \quad (1)$$

where  $n$  is the carrier density and  $k_2$  and  $k_3$  are the bimolecular and Auger rate coefficients, respectively. Global fits for all fluences at a given temperature are shown in Figure 2, these allow the  $k_2$  and  $k_3$  to be estimated at each temperature. Further details on the fitting are in the SI, as is a consideration of systematic error in the estimation of parameters at a given temperature caused by the different transient laser-pulse induced heating at the different excitation fluences.

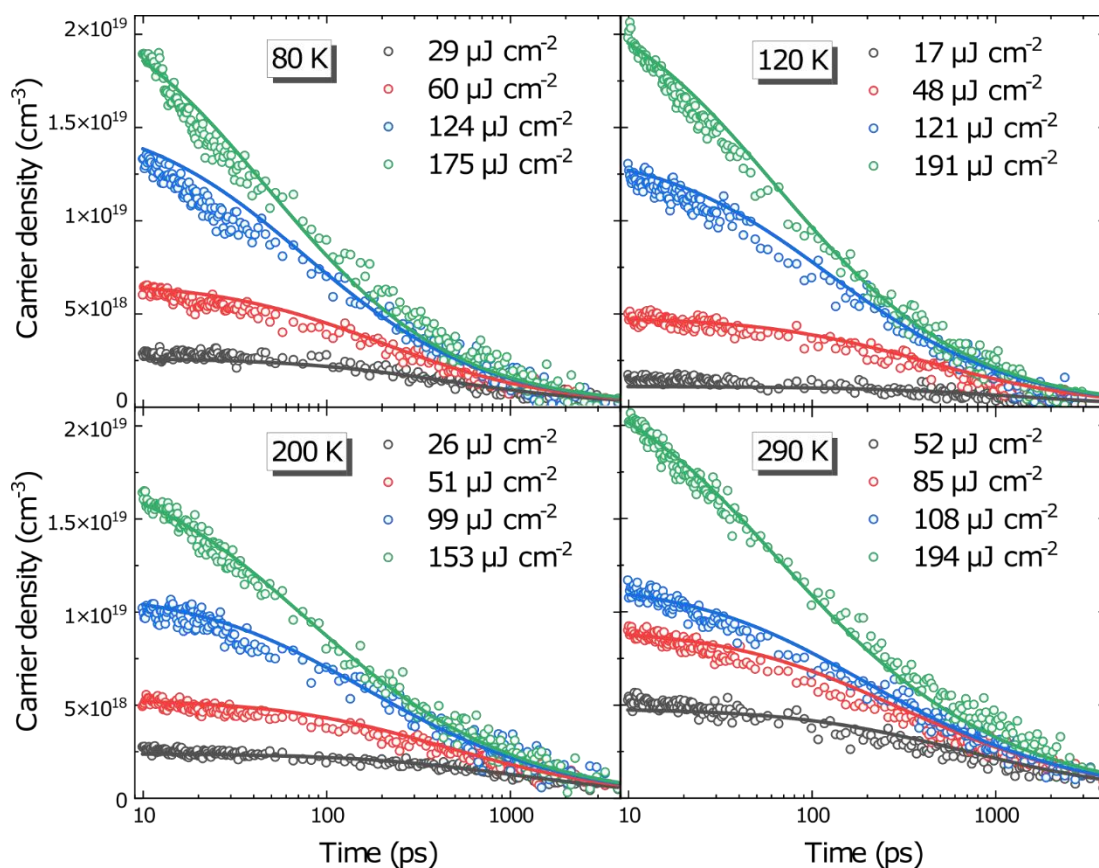


**Figure 2.** Carrier density as a function of time from 10 ps up to 4 ns for different initial carrier densities, at 80 K, 120 K, 200 K and 290 K. Open circles represent the measured data (integral of the transient reflection signal between 800 - 900 nm) and solid lines correspond to the global fitting based on bimolecular and Auger recombination as described in the text.

Figure 3 summarizes the extracted rate coefficients. The values for  $k_2$  and  $k_3$  are consistent with previous literature reports on other perovskite formulations (Table S1). The bimolecular rate coefficient decreases with increasing temperature, following the relation  $k_2 \propto T^{-3/2}$  (Figure 3a). This decrease is consistent with a reduction of the carrier mobility with increasing temperature, as theoretically expected due to increased phonon scattering,<sup>20,21</sup> and it is also consistent with the behaviour of reported values for MAPI.<sup>10,18,22,23</sup>

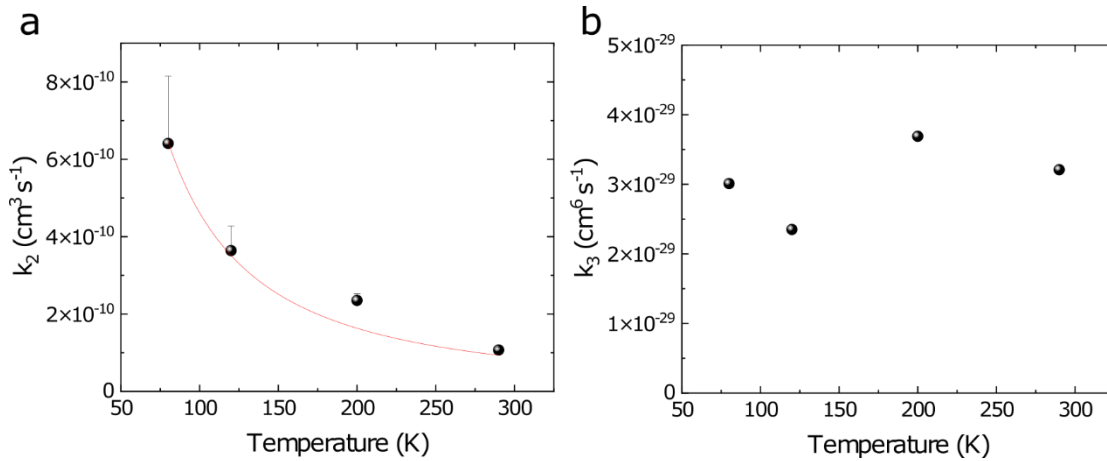


**Figure 3.** Recombination coefficients as a function of temperature extracted from the global fitting of the carrier recombination dynamics. Black spheres represent the bimolecular rate coefficient  $k_2$  (a) and the Auger coefficient  $k_3$  (b), and the red line corresponds to the power law dependence  $T^{-3/2}$ . Note that the error bars consider the heating effect from the pump (details are provided in the Supporting Information).

The Auger recombination is a third-order process, which depends highly on the electronic band structure.<sup>24–27</sup> The unexpectedly weak temperature dependence of the Auger coefficient is depicted in Figure 3b. Typically, the Auger coefficient in inorganic semiconductors increases with temperature.<sup>28–32</sup> In InGaAs, the Auger coefficient increases by a factor of two, from  $1.5 \cdot 10^{-28}$  cm<sup>6</sup> s<sup>-1</sup> at 200 K, to  $3 \cdot 10^{-28}$  cm<sup>6</sup> s<sup>-1</sup> at 300K.<sup>31</sup> In the same temperature range, the Auger coefficient for GaInAsP increases from  $4.01 \cdot 10^{-29}$  cm<sup>6</sup> s<sup>-1</sup> to  $5.9 \cdot 10^{-29}$  cm<sup>6</sup> s<sup>-1</sup>.<sup>32</sup> For metal halide perovskites, it has previously been established that the Auger coefficient shows a very strong dependency on the crystal phase. For the low-temperature-stable orthorhombic phase of MAPI, the Auger rate was found to decrease with increasing temperature, whereas for the room temperature-stable tetragonal phase the value stays approximately constant.<sup>18,33</sup> The triple cation perovskites under study here remain constantly in the cubic phase throughout the entire temperature range,<sup>9,34</sup> possibly

explaining the constant Auger rate from room to cryogenic temperature. The extracted Auger coefficients  $(3 \pm 0.7) \cdot 10^{-29} \text{ cm}^{-6} \text{ s}^{-1}$  are one to two orders of magnitude smaller than the previously reported for MAPI in the tetragonal phase.<sup>18</sup> Further work to elucidate how material chemistry alters the Auger rates in perovskites, and the temperature dependence thereof will be of interest.

The increase in ASE threshold as a function of temperature in MAPI has already been discussed by Jia *et al.*<sup>10</sup>, in terms of energy dispersion of the charge carriers in shallow band tails. This approach leads to a prediction for the threshold as a function of temperature,  $N_{th} \propto T^3 [\cot^2(k_b T \pi / E_0) + 1]$ .<sup>10,35</sup> where  $E_0$  is the characteristic decay. We also find that this function provides a reasonable parameterization of the ASE threshold as a function of temperature and extract  $E_0 = 44$  meV (similar the 39 meV reported for MAPI).<sup>9,10</sup> However, in the following, we examine in more detail how the changing rates of bimolecular and Auger recombination alongside the energy dilution (quantified below in terms of the fraction of the total emission within the ASE band) can explain the temperature dependence of the ASE threshold.

The carrier density,  $N_A$ , at which the Auger and bimolecular free carrier recombination rates become equal can be determined using  $k_2 = k_3 \cdot N_A$ . At carrier densities higher than  $N_A$ , Auger recombination will be faster than bimolecular free carrier recombination, and the Auger recombination will significantly increase the ASE threshold. In Figure 4a, we compare  $N_A$  with the ASE threshold density (determined for the reference samples in Figure 1). the ASE threshold is below  $N_A$  at temperatures below 250 K but the rate of Auger recombination exceeds the rate of bimolecular recombination at the threshold density above 250 K.

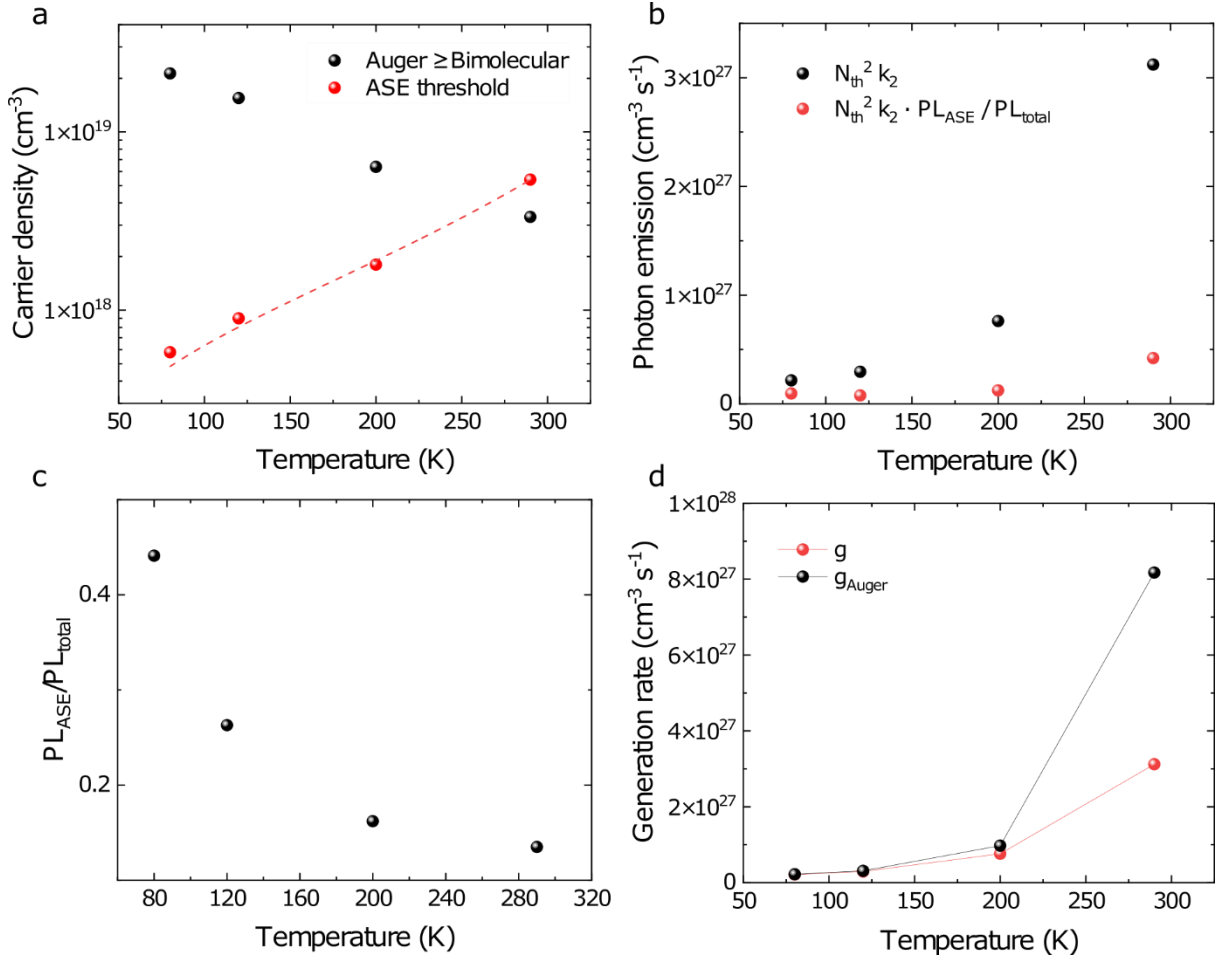


**Figure 4.** Influence of recombination coefficients on ASE as a function of temperature. Carrier density at which the bimolecular and Auger recombination become equal (black spheres) and ASE threshold carrier density (red spheres) (a). The red dashed line shows the band tail fit. The total rate of photon emission (black spheres) and the rate of photon emission within the ASE band (red spheres) (b). The fraction of the PL emission originating from the ASE band, given as the ratio of the PL in the ASE band to the total PL (c). Generation rate for the CW steady-state condition, including (black spheres,  $g_{Auger}$ ) and neglecting (red spheres,  $g$ ) the Auger recombination (d).

To sustain ASE, the product of the photon and carrier density need to reach a critical value. To achieve the necessary photon density, the rate of emission per volume at photon wavelengths within the ASE band must reach a critical value. Although the lasing threshold for films with

photonic structures will be lower than the ASE threshold due to the effects on the photon density through modified emission rate and light confinement (and this reduction is important for achieving room-temperature or electrically-pumped lasing, see Table S2 for comparison of lasing thresholds in various structures), the study of the ASE gives a clearer insight into the intrinsic gain properties of the material. The total rate of photon emission per volume at the ASE threshold density as a function of temperature,  $k_2(T)N_{th}(T)^2$  is plotted in Figure 4b. The rate of photon emission necessary to reach the ASE threshold increases sharply with temperature because the full-width at half maximum of the spontaneous PL spectra broadens significantly with increasing temperature. The fraction of the spontaneous PL that lies within the ASE bandwidth consequently decreases with increasing temperature. Figure S7 demonstrates how the fraction of the spontaneous PL within the ASE band can be determined, and this fraction is presented in Figure 4c. The rate of photon emission into the ASE band at the threshold is found by multiplying the total photon emission rate ( $k_2N_{th}^2$ ) by the fraction of the photon emission in the ASE band ( $PL_{ASE}/PL_{total}$ ) (red points in Figure 4b). The rate of photon emission into the ASE band stays constant, as we would expect (at least at temperatures under 200 K, the small increase at higher temperatures could be due to slightly increased photon loss at high temperatures). Thus, we can reach the strong conclusion that below 200 K, ASE in our materials requires a photon emission rate of approximately  $10^{26} \text{ cm}^{-3} \text{ s}^{-1}$  into the ASE band (Figure 4b); and the temperature dependence of the ASE threshold is due to: (1) the change in the rate of photon emission due to the temperature dependence of  $k_2$ , and (2) the change in the fraction of PL that is emitted into the ASE band due to the broadening of the PL spectrum with increasing temperature. Both of these effects play significant roles in the increase of the ASE threshold with increasing temperature under 200 K. Auger recombination, however, does not play a major role in this temperature range.

To more clearly show the effect of the Auger process on thresholds, we consider the steady-state generation rate needed to reach the threshold density with and without Auger recombination. The generation rate considering Auger processes is  $g_{Auger} = k_2n^2 + k_3n^3$  whereas that without Auger processes considered is  $g = k_2n^2$ . It can be seen in Figure 4d that  $g_{Auger}$  and  $g$  are almost identical until 200 K, after which  $g_{Auger}$  starts to significantly exceed  $g$ .

In summary, below 200 K, the rapid increase in threshold with temperature is related to: 1) the decrease in  $k_2$  with temperature leading higher carrier densities to be required to maintain the same total emission rate, and 2) the broadening of the PL spectrum decreasing the fraction of PL involved with the ASE. Above 200 K, Auger recombination can also affect the threshold. Under the pulsed conditions studied here,  $k_1$  can be neglected but Jia *et al.*,<sup>10</sup> have established that  $k_1$  can increase by a photo-induced process until it is no longer negligible under quasi-CW excitation. This certainly could further affect the CW ASE and lasing thresholds, on top of the considerations presented herein. To increase the temperature at which CW ASE can be maintained, material strategies to maintain a higher  $k_2$  and narrower PL bandwidth at higher temperatures should be examined. This may involve tailoring the electron-phonon interactions through strain or rigidifying the perovskite via matrix materials.

## ASSOCIATED CONTENT

### **Supporting Information.**

The following files are available free of charge. Emission spectra for sapphire and Si substrates, details on global fit, influence of pump-induced heating, justification for neglecting SRH, comparison of emission rates with other perovskites, comparison of lasing/ASE thresholds for different photonic structures, fraction of PL in the ASE band, experimental methods. (PDF)

## AUTHOR INFORMATION

### Notes

The authors declare no competing financial interests.

### ACKNOWLEDGMENT

The authors gratefully acknowledge funding from the DFG (PEROLAS, funding code: 409035484), the Karlsruhe School of Optics & Photonics (KSOP), the Helmholtz Energy Materials Foundry (HEMF), and the Excellence Cluster “3D Matter Made to Order” (3DMM2O).

### REFERENCES

- (1) Sutherland, B. R.; Sargent, E. H. Perovskite Photonic Sources. *Nat. Photonics* **2016**, *10* (5), 295–302. <https://doi.org/10.1038/nphoton.2016.62>.
- (2) Evans, T. J. S.; Schlaus, A.; Fu, Y.; Zhong, X.; Atallah, T. L.; Spencer, M. S.; Brus, L. E.; Jin, S.; Zhu, X.-Y. Continuous-Wave Lasing in Cesium Lead Bromide Perovskite Nanowires. *Adv. Opt. Mater.* **2018**, *6* (2), 1700982. <https://doi.org/10.1002/adom.201700982>.
- (3) Su, R.; Diederichs, C.; Wang, J.; Liew, T. C. H.; Zhao, J.; Liu, S.; Xu, W.; Chen, Z.; Xiong, Q. Room-Temperature Polariton Lasing in All-Inorganic Perovskite Nanoplatelets. *Nano Lett.* **2017**, *17* (6), 3982–3988. <https://doi.org/10.1021/acs.nanolett.7b01956>.
- (4) Qin, C.; Sandanayaka, A. S.; Zhao, C.; Matsushima, T.; Zhang, D.; Fujihara, T.; Adachi, C. Stable Room-Temperature Continuous-Wave Lasing in Quasi-2D Perovskite Films. *Nature* **2020**, *585*, 53. <https://doi.org/10.1038/s41586-020-2621-1>.
- (5) Brenner, P.; Paetzold, U. W.; Turnbull, G. A.; Giebink, N. C.; Samuel, I. D. W.; Lemmer,

- U.; Howard, I. A. Comment on “Room-Temperature Continuous-Wave Operation of Organometal Halide Perovskite Lasers.” *ACS Nano*. American Chemical Society November 26, 2019, pp 12257–12258. <https://doi.org/10.1021/acsnano.9b00133>.
- (6) Li, Z.; Moon, J.; Gharajeh, A.; Haroldson, R.; Hawkins, R.; Hu, W.; Zakhidov, A.; Gu, Q. Room-Temperature Continuous-Wave Operation of Organometal Halide Perovskite Lasers. *ACS Nano* **2018**, *12* (11), 10968–10976. <https://doi.org/10.1021/acsnano.8b04854>.
- (7) Jia, Y.; Kerner, R. A.; Grede, A. J.; Rand, B. P.; Giebink, N. C. Continuous-Wave Lasing in an Organic–Inorganic Lead Halide Perovskite Semiconductor. *Nat. Photonics* **2017**, *11* (12), 784–788. <https://doi.org/10.1038/s41566-017-0047-6>.
- (8) Saliba, M.; Matsui, T.; Seo, J.-Y.; Domanski, K.; Correa-Baena, J.-P.; Nazeeruddin, M. K.; Zakeeruddin, S. M.; Tress, W.; Abate, A.; Hagfeldt, A.; Grätzel, M. Cesium-Containing Triple Cation Perovskite Solar Cells: Improved Stability, Reproducibility and High Efficiency. *Energy Environ. Sci.* **2016**, *9* (6), 1989–1997. <https://doi.org/10.1039/C5EE03874J>.
- (9) Brenner, P.; Bar-On, O.; Jakoby, M.; Allegro, I.; Richards, B. S.; Paetzold, U. W.; Howard, I. A.; Scheuer, J.; Lemmer, U. Continuous Wave Amplified Spontaneous Emission in Phase-Stable Lead Halide Perovskites. *Nat. Commun.* **2019**, *10* (1). <https://doi.org/10.1038/s41467-019-08929-0>.
- (10) Jia, Y.; Kerner, R. A.; Grede, A. J.; Rand, B. P.; Giebink, N. C. Factors That Limit Continuous-Wave Lasing in Hybrid Perovskite Semiconductors. *Adv. Opt. Mater.* **2020**, *8* (2), 1901514. <https://doi.org/10.1002/adom.201901514>.
- (11) Haugeneder, A.; Neges, M.; Kallinger, C.; Spirkl, W.; Lemmer, U.; Feldmann, J.; Amann, M. C.; Scherf, U. Nonlinear Emission and Recombination in Conjugated Polymer

- Waveguides. *J. Appl. Phys.* **1999**, *85* (2), 1124–1130. <https://doi.org/10.1063/1.369237>.
- (12) Pasanen, H. P.; Vivo, P.; Canil, L.; Abate, A.; Tkachenko, N. Refractive Index Change Dominates the Transient Absorption Response of Metal Halide Perovskite Thin Films in the near Infrared. *Phys. Chem. Chem. Phys.* **2019**, *21* (27), 14663–14670. <https://doi.org/10.1039/C9CP02291K>.
- (13) Yang, Y.; Yan, Y.; Yang, M.; Choi, S.; Zhu, K.; Luther, J. M.; Beard, M. C. Low Surface Recombination Velocity in Solution-Grown CH<sub>3</sub>NH<sub>3</sub>PbBr<sub>3</sub> Perovskite Single Crystal. *Nat. Commun.* **2015**, *6* (1), 7961. <https://doi.org/10.1038/ncomms8961>.
- (14) Halsall, M. P.; Crowe, I. F.; Mullins, J.; Oliver, R. A.; Kappers, M. J.; Humphreys, C. J. Photomodulated Reflectivity Measurement of Free-Carrier Dynamics in InGaN/GaN Quantum Wells. *ACS Photonics* **2018**, *5* (11), 4437–4446. <https://doi.org/10.1021/acsp Photonics.8b00904>.
- (15) Bennett, B. R.; Soref, R. A.; Del Alamo, J. A. Carrier-Induced Change in Refractive Index of InP, GaAs, and InGaAsP. *IEEE J. Quantum Electron.* **1990**, *26* (1), 113–122. <https://doi.org/10.1109/3.44924>.
- (16) Bulutay, C.; Turgut, C. M.; Zakhleniuk, N. A. Carrier-Induced Refractive Index Change and Optical Absorption in Wurtzite InN and GaN: Full-Band Approach. *Phys. Rev. B - Condens. Matter Mater. Phys.* **2010**, *81* (15), 1–10. <https://doi.org/10.1103/PhysRevB.81.155206>.
- (17) Auston, D. H. Picosecond Spectroscopy of Semiconductors. *Inst Phys Conf Ser* **1979**, No. 43, 73–82. <https://doi.org/10.11470/oubutsu1932.52.951>.
- (18) Milot, R. L.; Eperon, G. E.; Snaith, H. J.; Johnston, M. B.; Herz, L. M. Temperature-Dependent Charge-Carrier Dynamics in CH<sub>3</sub>NH<sub>3</sub>PbI<sub>3</sub> Perovskite Thin Films. *Adv.*

- Funct. Mater.* **2015**, 25 (39), 6218–6227. <https://doi.org/10.1002/adfm.201502340>.
- (19) Richter, J. M.; Abdi-Jalebi, M.; Sadhanala, A.; Tabachnyk, M.; Rivett, J. P. H.; Pazos-Outón, L. M.; Gödel, K. C.; Price, M.; Deschler, F.; Friend, R. H. Enhancing Photoluminescence Yields in Lead Halide Perovskites by Photon Recycling and Light Out-Coupling. *Nat. Commun.* **2016**, 7. <https://doi.org/10.1038/ncomms13941>.
- (20) Aigrain, P. Recombination Processes in Semiconductors. *Nuovo Cim. Ser. 10* **1958**, 7 (2 Supplement), 724–729. <https://doi.org/10.1007/BF02751505>.
- (21) Lasher, G.; Stern, F. Spontaneous and Stimulated Recombination Radiation in Semiconductors. *Phys. Rev.* **1964**, 133 (2A), A553–A563. <https://doi.org/10.1103/PhysRev.133.A553>.
- (22) Davies, C. L.; Filip, M. R.; Patel, J. B.; Crothers, T. W.; Verdi, C.; Wright, A. D.; Milot, R. L.; Giustino, F.; Johnston, M. B.; Herz, L. M. Bimolecular Recombination in Methylammonium Lead Triiodide Perovskite Is an Inverse Absorption Process. *Nat. Commun.* **2018**, 9 (1), 293. <https://doi.org/10.1038/s41467-017-02670-2>.
- (23) Herz, L. M. Charge-Carrier Mobilities in Metal Halide Perovskites: Fundamental Mechanisms and Limits. *ACS Energy Lett.* **2017**, 2 (7), 1539–1548. <https://doi.org/10.1021/acsenergylett.7b00276>.
- (24) Even, J.; Pedesseau, L.; Jancu, J. M.; Katan, C. Importance of Spin-Orbit Coupling in Hybrid Organic/Inorganic Perovskites for Photovoltaic Applications. *J. Phys. Chem. Lett.* **2013**, 4 (17), 2999–3005. <https://doi.org/10.1021/jz401532q>.
- (25) Even, J.; Pedesseau, L.; Katan, C.; Kepenekian, M.; Lauret, J.-S.; Saponi, D.; Deleporte, E. Solid-State Physics Perspective on Hybrid Perovskite Semiconductors. *J. Phys. Chem. C* **2015**, 119 (19), 10161–10177. <https://doi.org/10.1021/acs.jpcc.5b00695>.

- (26) Pham, H. T.; Duong, T.; Weber, K. J.; Wong-Leung, J. Insights into Twinning Formation in Cubic and Tetragonal Multi-Cation Mixed-Halide Perovskite. *ACS Mater. Lett.* **2020**, *2* (4), 415–424. <https://doi.org/10.1021/acsmaterialslett.0c00083>.
- (27) Ščajev, P.; Litvinas, D.; Soriū Tė, V.; Kreiza, G.; Stanionytė, S.; Jursėnas, S. Crystal Structure Ideality Impact on Bimolecular, Auger, and Diffusion Coefficients in Mixed-Cation Cs XMA1- XPbBr<sub>3</sub> and Cs XFA1- XPbBr<sub>3</sub> Perovskites. *J. Phys. Chem. C* **2019**, *123* (39). <https://doi.org/10.1021/acs.jpcc.9b05824>.
- (28) Dutta, N. K.; Nelson, R. J. The Case for Auger Recombination in In<sub>1-x</sub>Ga<sub>x</sub>As<sub>y</sub>P<sub>1-y</sub>. *J. Appl. Phys.* **1982**, *53* (1), 74–92. <https://doi.org/10.1063/1.329942>.
- (29) Huld, L.; Nilsson, N. G.; Svantesson, K. G. The Temperature Dependence of Band-to-Band Auger Recombination in Silicon. *Appl. Phys. Lett.* **1979**, *35* (10), 776–777. <https://doi.org/10.1063/1.90974>.
- (30) Svantesson, K. G.; Nilsson, N. G. The Temperature Dependence of the Auger Recombination Coefficient of Undoped Silicon. *J. Phys. C Solid State Phys.* **1979**, *12* (23), 5111–5120. <https://doi.org/10.1088/0022-3719/12/23/019>.
- (31) Hausser, S.; Fuchs, G.; Hangleiter, A.; Streubel, K.; Tsang, W. T. Auger Recombination in Bulk and Quantum Well InGaAs. *Appl. Phys. Lett.* **1990**, *56* (10), 913–915. <https://doi.org/10.1063/1.103175>.
- (32) Casey, H. C. Temperature Dependence of the Threshold Current Density in InP-Ga<sub>0.28</sub>In<sub>0.72</sub>As<sub>0.6</sub>P<sub>0.4</sub> ( $\Lambda=1.3$  Mm) Double Heterostructure Lasers. *J. Appl. Phys.* **1984**, *56* (7), 1959–1964. <https://doi.org/10.1063/1.334226>.
- (33) Trimpl, M. J.; Wright, A. D.; Schutt, K.; Buizza, L. R. V.; Wang, Z.; Johnston, M. B.; Snaith, H. J.; Müller-Buschbaum, P.; Herz, L. M. Charge-Carrier Trapping and Radiative

- Recombination in Metal Halide Perovskite Semiconductors. *Adv. Funct. Mater.* **2020**, *30* (42), 2004312. <https://doi.org/10.1002/adfm.202004312>.
- (34) Moghadamzadeh, S.; Hossain, I. M.; Jakoby, M.; Abdollahi Nejad, B.; Rueda-Delgado, D.; Schwenzer, J. A.; Gharibzadeh, S.; Abzieher, T.; Khan, M. R.; Haghighirad, A. A. *et al.* Spontaneous Enhancement of the Stable Power Conversion Efficiency in Perovskite Solar Cells. *J. Mater. Chem. A* **2020**, *8* (2), 670–682. <https://doi.org/10.1039/c9ta09584e>.
- (35) Adams, M. J. Theoretical Effects of Exponential Band Tails on the Properties of the Injection Laser. *Solid. State. Electron.* **1969**, *12* (8), 661–669. [https://doi.org/10.1016/0038-1101\(69\)90038-0](https://doi.org/10.1016/0038-1101(69)90038-0).